A Myoelectric Control Interface for Upper-Limb Robotic Rehabilitation Following Spinal Cord Injury

Craig G. McDonald, *Student Member, IEEE*, Jennifer L. Sullivan, Troy A. Dennis, *Student Member, IEEE*, and Marcia K. O'Malley, *Fellow, IEEE*

***Abstract*—Spinal cord injury (SCI) is a widespread, life-altering injury leading to impairment of sensorimotor function that, while once thought to be permanent, is now being treated with the hope of one day being able to restore function. Surface electromyography (EMG) presents an opportunity to examine and promote human engagement at the neuromuscular level, enabling new protocols for intervention that could be combined with robotic rehabilitation, particularly when robot motion or force sensing may be unusable due to the user's impairment. In this paper, a myoelectric control interface to an exoskeleton for the elbow and wrist was evaluated on a population of ten able-bodied participants and four individuals with cervical-level SCI. The ability of an EMG classifier to discern intended direction of motion in single-degree-of-freedom (DoF) and multi-DoF control modes was assessed for usability in a therapy-like setting. The classifier demonstrated high accuracy for able-bodied participants (averages over 99% for single-DoF and near 90% for multi-DoF), and performance in the SCI group was promising, warranting further study (averages ranging from 85% to 95% for single-DoF, and variable multi-DoF performance averaging around 60%). These results are encouraging for the future use of myoelectric interfaces in robotic rehabilitation for SCI.**

***Index Terms*—Rehabilitation robotics, spinal cord injury, electromyography, myoelectric control, pattern recognition.**

I. Introduction

SPINAL cord injury (SCI) is a life-altering injury that currently affects hundreds of thousands of individuals in the U.S [1]. These injuries are usually caused by mechanical trauma somewhere along the spinal cord, which disrupts both sensation and motor function at and below the level of injury. The resulting impairment depends largely on the severity of the injury and can range from some muscle weakness to complete paralysis. While the effects of spinal injury were once considered more or less permanent, scientific advancements of the past several decades have dramatically changed outlooks to the point that recovery of motor function is now believed to be an attainable goal for the future of treatment [2].

Robotic rehabilitation has been demonstrated to be an effective therapy to promote motor recovery [3]. However, for the therapy to be most effective, it must be intensive, and patients must be appropriately challenged and mentally engaged [4], [5]. For rehabilitation robots, this is typically addressed with some type of shared control, where the device monitors the user's effort through movement or force sensing and then gauges how much assistance to provide. Such a robotic system has limited ability to respond appropriately when the patient has very little movement capability.

Surface electromyography (EMG) – the indirect measurement of muscle contraction force from the change in electric potential occurring locally at the skin surface – provides an opportunity to examine and promote human engagement at the neuromuscular level, allowing for new protocols for intervention with robotic rehabilitation. Even in the absence of robotic assistance, EMG-triggered neuromuscular stimulation has been shown to be an effective treatment for stroke recovery [6]. Based on sensorimotor integration theory [7], when a patient generates muscle activity above a certain threshold, as detected by EMG, then an assistive electrical stimulus is applied to the muscles. Critically, movement-related afferent signals are synchronized with volitional muscle contraction from intended movement [8]. In this work, we present a robotic rehabilitation system with the same principle of operation, but with robotic assistance replacing the electrical stimulus. Such a system is likely to be found engaging for the user, and to enhance motor learning [9], by synchronizing consciously generated EMG with proprioceptive feedback.

If we consider a hypothetical user who is very weak in a certain degree of freedom (Dof), an EMG-controlled exoskeleton could tailor its response to the user's effort as they merely attempt to generate motion, whereas a velocity or force-triggered exoskeleton could not. Such a user could find the initial trigger challenging and moving through the full trajectory impossible. Here, we would argue that EMG-triggered assistance is still engaging, even though the robot is following a predefined trajectory after the

Manuscript received August 12, 2019; revised January 31, 2020; accepted March 5, 2020. Date of publication March 10, 2020; date of current version April 8, 2020. This work was supported by Mission Connect, a project of the TIRR Foundation under Award 018-114. *(Corresponding author: Craig G. McDonald.)*

Craig G. McDonald, Jennifer L. Sullivan, and Troy A. Dennis were with the Department of Mechanical Engineering, Rice University, Houston, TX 77005-1892 USA (e-mail: craig.g.mcdonald@gmail.com).

Marcia K. O'Malley is with the Department of Mechanical Engineering, Rice University, Houston, TX 77005-1892 USA.

Digital Object Identifier 10.1109/TNSRE.2020.2979743

1534-4320 © 2020 IEEE. Personal use is permitted, but republication/redistribution requires IEEE permission. See https://www.ieee.org/publications/rights/index.html for more information.

Authorized licensed use limited to: Fondren Library Rice University. Downloaded on April 10,2020 at 14:20:43 UTC from IEEE Xplore. Restrictions apply.

initial trigger. Moreover, an EMG-based control algorithm could allow therapists to train specific muscle coordination strategies to promote healthy movement synergies and avoid reinforcing any maladaptive activation patterns that patients might be utilizing. The potential value of EMG control is furthered by the fact that many individuals with SCI still exhibit significant myoelectric activity in their affected limbs, even if they have little to no volitional control over those muscles [10], [11].

However, accurately decoding high-level motor intention is still a significant challenge, given the inherent noisiness and sensitivity of EMG measurements as well as the complexity of the neuromusculoskeletal system. Even among healthy, able-bodied individuals, differences in EMG patterns between users are significant enough that most systems need to be calibrated for each individual user. Potential user motor impairment only adds to this challenge, as the patterns of the myoelectric signal are expected to be atypical [12].

Despite these challenges, a number of research groups have been successful in developing myoelectric control interfaces, particularly for robotic prostheses. In the seminal work by Hudgins [13], a short time window of the myoelectric signal was transformed into a set of features, which was then used to classify different types of contractions of the amputee's upper limb. Work on myoelectric control interfaces for the upper limb has largely consisted of incremental improvements to Hudgins' approach, with notable difficulty in achieving accurate discrimination of multiple-degree-of-freedom movements [14]. In another example by Englehart and Hudgins, they demonstrated a real-time control scheme that could accurately discriminate between four different hand-wrist poses from four channels of myoelectric data using linear discriminant analysis (LDA), a standard classification algorithm in machine learning that is often preferred for its simplicity and robustness [15].

We have transferred the myoelectric control strategy for robotic prostheses to our robotic exoskeleton for rehabilitation, the MAHI Exo-II, shown in Fig. 1. The MAHI Exo-II is an upper-limb exoskeleton for the elbow and wrist joints that allows for isolated or coordinated movements across four anatomical degrees of freedom (DoF): elbow flexion/extension (E-Flx/Ext), forearm pronation/supination (F-Pro/Sup), wrist flexion/extension (W-Flx/Ext), and wrist radial/ulnar deviation (W-Rad/Uln). The myoelectric interface records the activity of eight muscles that control the elbow, forearm, and wrist, from which the intended direction of movement is classified using LDA.

The target population for our system is individuals that have been affected by spinal injury, where the muscles themselves are present and intact, but damage to the corticospinal tract inhibits the ability of the central nervous system to actuate them. Similar work has already been carried out by Lu *et al.* [16] for the control of a robotic exoskeleton for the hand. In a study that included two SCI participants, they successfully achieved real-time control with a high degree of accuracy, demonstrating the potential for EMG-controlled devices in robotic rehabilitation following spinal injury.

Fig. 1. The MAHI Exo-II rehabilitation exoskeleton, capable of providing independent joint torques for four anatomical degrees of freedom. This user's arm is fitted with surface EMG electrodes at eight locations covering muscles that control the elbow and wrist.

We aim to demonstrate that these myoelectric control schemes can naturally be extended to the control of our robotic exoskeleton for the elbow and wrist, the MAHI Exo-II, for the target population of SCI. With incomplete cervical SCI individuals we have used LDA – trained to recognize EMG patterns generated by different user intentions – to then successfully predict the user's intended direction of motion. No constraints were imposed on the specific EMG patterns themselves, except that they be consistent and distinguishable from one another. This allows us to demonstrate the existence of consistent mappings between user intention and EMG patterns, independent of any attempt to change the participant's muscle activity beyond their initial capabilities.

This paper focuses on the design of the classification algorithm to decode single- and multi-DoF movement intent from EMG signals. We present the results of a study characterizing its performance in both individuals with SCI and able-bodied control participants.

II. Methods

A. Myoelectric Classifier Design

The myoelectric control interface was designed to operate in six control modes: four single-DoF, corresponding to the active degrees of freedom of the exoskeleton, and two multi-DoF. The single-DoF modes were elbow flexion/extension (E-Flx/Ext), forearm pronation/supination (F-Pro/Sup), wrist flexion/extension (W-Flx/Ext), and wrist radial/ulnar deviation (W-Rad/Uln). The multi-DoF modes were elbow flexion/extension combined with forearm pronation/supination (EF-Multi) and wrist flexion/extension combined with wrist radial/ulnar deviation (WW-Multi). For each control mode, an LDA classifier was trained to predict the direction of the user's intended movement using features of the myoelectric signal collected during a brief isometric contraction. For each single-DoF mode, there were two possible classification

Authorized licensed use limited to: Fondren Library Rice University. Downloaded on April 10,2020 at 14:20:43 UTC from IEEE Xplore. Restrictions apply.

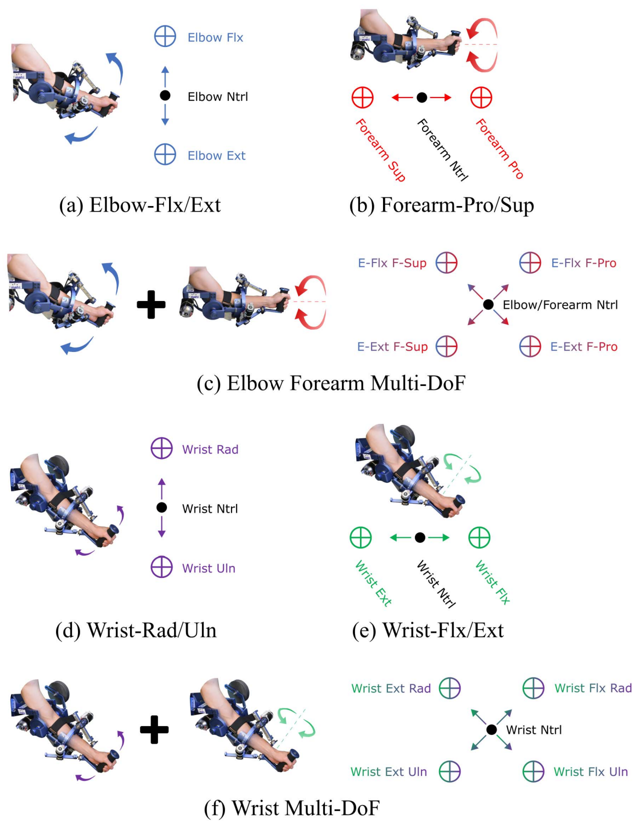

Fig. 2. Visual representation of the task for the two single-DoF modes (a) elbow flexion/extension (E-Flx/Ext) and (b) forearm pronation/supination (F-Pro/Sup), their combination (c) in a multi-DoF mode (EF-Multi), the two single-DoF modes (d) wrist radial/ulnar deviation (W-Rad/Uln), (e) wrist flexion/extension (W-Flx/Ext), and their combination (f) in a multi-DoF mode (WW-Multi). Labeled targets with arrows represent the graphical user interface that the users were shown, which was automatically adjusted for each control mode.

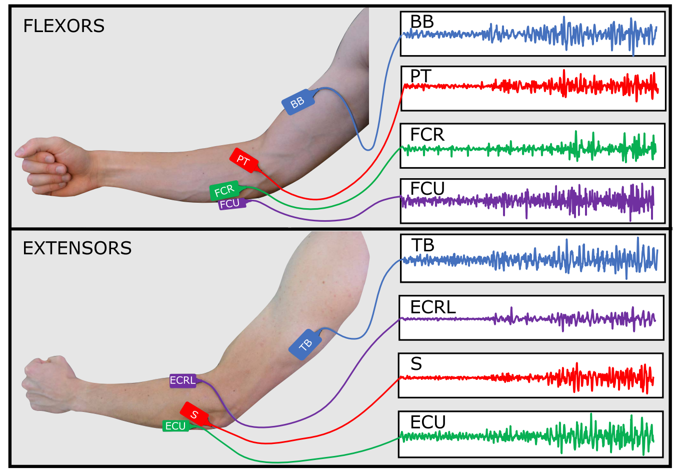

Fig. 3. Approximate locations for each EMG electrode labeled by muscle. Muscles that contribute primarily to E-Flx/Ext are marked in blue, F-Pro/Sup in red, W-Flx/Ext in green, and W-Rad/Uln in purple. The right portion of the figure shows examples of filtered EMG waveforms from an isometric contraction in the Elbow-Forearm multi-DoF mode.

directions, and for each multi-DoF mode, there were four possible classification directions, shown in Fig. 2.

1) Myoelectric Feature Collection: Myoelectric signals were recorded from eight muscles that control movements at the elbow, forearm, and wrist: biceps brachii (BB), triceps brachii (TB), pronator teres (PT), supinator (S), flexor carpi radialis (FCR), extensor carpi ulnaris (ECU), extensor carpi radialis longus (ECRL), and flexor carpi ulnaris (FCU). These muscles were chosen based on the experiment performed by Gopura and Kiguchi [17] to minimize the noise and cross-talk associated with overlapping muscles. Their approximate positions are shown in Fig. 3 [18]. Analog band-pass filtering was applied to each channel at 20 Hz–450 Hz by the Delsys Bagnoli EMG system, removing movement artifacts. All channels were then sampled at 1 kHz, and additional digital band-pass filtering was applied (Butterworth, 4th order, 20 Hz–450 Hz), removing the signal mean. No additional signal processing was applied before feature extraction.

The standard time-domain (TD) features originally introduced by Hudgins in [13] were computed from the myoelectric signal, augmented with the autoregressive (AR) coefficients and the root-mean-square (RMS), both of which are popular choices as additions to the TD feature set and have been shown to increase classification accuracy [19], [20]. The time domain features are number of zero crossings (ZC), mean absolute value (MAV), waveform length (WL), and number of slope sign changes (SSC) (formulas found in [13].) The coefficients of a fourth-order autoregressive model (AR1–4) capture the frequency content of the time-varying myoelectric signal. The total feature set (4TD+4AR+RMS) included nine features to be calculated on each channel. The TD and RMS features were normalized by the average value of all channels [16].

Features were computed from a 200 ms window of data at the onset of each contraction. This time span was chosen in accordance with the findings of Smith *et al.* [21] to balance the competing effects of classification error and controller delay.

2) Classifier Fitting & Customization: Classifiers were trained using an iterative combination of linear discriminant analysis (LDA) to fit the data and Recursive Feature Elimination with Cross Validation (RFECV) to reduce the feature set. Both algorithms were implemented by the Scikit-Learn toolbox in Python. LDA was chosen for its relative simplicity and high success rate when compared to other common myoelectric classification algorithms, and its ability to successfully make classification predictions with a low amount of training data [14]. RFECV is an algorithm that uses cross validation on the set of training data it has been given in order to select the optimum feature combination, often resulting in a significantly smaller number of features being used for classification. Although the full feature set can be used without reduction, it has been shown that using a smaller subset of features for classification can improve or maintain classifier performance while reducing computation time [22].

B. Study Design

The main objective of this study was to generate a unique classifier for each participant and each control mode to compare the performance between single-DoF and multi-DoF modes and between able-bodied and SCI participants. For each case (i.e., participant and control mode), the protocol

Authorized licensed use limited to: Fondren Library Rice University. Downloaded on April 10,2020 at 14:20:43 UTC from IEEE Xplore. Restrictions apply.

Fig. 4. An illustration of the experimental task, as experienced by the user, for the single-DoF elbow flexion/extension control mode. The user is held in a neutral position by the exoskeleton as they attempt to generate movement about the selected degree(s) of freedom, received commands from the visual interface. For each mode, targets are presented in a random order, with the user generating an isometric contraction during an "active" phase, and then relaxing their muscles during a "rest" phase. Once the threshold for detection of myoelectric activity is set during the calibration step, the training data is collected in the manner depicted here for the necessary number of trials, and a classifier is fit to the training data. Then, predictions made by the classifier are tested also in the manner that is depicted here; i.e., it is the same as the collection of training data, from the user's perspective. Finally, the classifier predictions are testing with the robot carrying the user to the predicted target and back after the "active" phase of each trial.

TABLE I
SCI PARTICIPANT INFORMATION

	Sex	Age	Level	Severity
SCI 1	F	30	C5/6	ASIA-B
SCI 2	M	22	C4/5/6	ASIA-C
SCI 3	M	23	C6	ASIA-A
SCI 4	M	49	C3/4/5	ASIA-C

was broken into three stages: calibration of active contraction versus rest states; training data collection and classifier fitting; and online testing of classifier performance. Fig. 4 illustrates the task from the user's perspective. By testing classifier performance online with individuals from the target population wearing a rehabilitation exoskeleton, we are emulating the conditions of the intended application.

C. Participants

Ten able-bodied individuals participated, one female and nine male, ages 20–28. Four individuals with SCI participated; details are given in TABLE I. (Rice University IRB protocol FY2018-29.) For SCI, the extent of injury is quantifiable by the American Spinal Injury Association's (ASIA) impairment scale, with grade A corresponding to a complete injury with loss of sensory and motor function below the level of injury, and grades B-D describing degrees of incomplete injury from most to least severe. Participants' location of injury, identified by segments of the spinal column, was restricted to be cervical (C) level for this study, and ranged from level C3 down to C6, meaning impairment of wrist function would be present as well as probable impairment of elbow function.

D. Hardware

The MAHI Exo-II, shown in Fig. 1, is a robotic exoskeleton designed for the rehabilitation of the elbow and wrist joints [23]. It features serially connected joints for elbow flexion/extension (E-Flx/Ext) and forearm pronation/supination (F-Pro/Sup) joints, and a parallel revolute-prismatic-spherical mechanism that achieves wrist flexion/extension (W-Flx/Ext) and wrist radial/ulnar deviation (W-Rad/Uln). The exoskeleton is equipped with an adjustable counterweight for passive gravity compensation of the elbow joint. In all phases of the experiment, the robot was position-controlled with proportional-derivative feedback. When robot motion feedback was provided, the robot followed a pre-programmed reference trajectory.

The Delsys Bagnoli EMG system provides eight channels of surface EMG data. The variable gain for the channel amplification was set to 1000. All robot and EMG data was acquired with the Quanser Q8-USB, sampled at 1 kHz, and band-pass filtered at 20 Hz–450 Hz.

E. Experimental Protocol

1) Setup: EMG electrodes were placed according to SENIAM guidelines [24], Fig. 3. Neoprene wrapping was used to insulate the EMG electrodes from the metal of the exoskeleton and the electrical interference from the motors (the neoprene wrapping is not shown in Fig. 1).

The height and shoulder abduction angle of the MAHI-Exo II were adjusted so the participant could hold their arm in a natural position with the elbow flexed while seated. The position of the chair relative to the exoskeleton was adjusted to keep both shoulders at equal heights and to keep the shoulder in the scapular plane ($\sim 30°$ from the frontal plane). Participants were instructed not to move their torsos or shoulders during testing but restraints were not used to enforce this. The wrist handle location was positioned to provide a maximum range of motion while the participant held it in a natural grip. The elbow joint counterweight was set so that the participant was able to be at rest while the robot elbow joint was at 90° of flexion.

The exoskeleton can be configured for left and right handed individuals, so the dominant arm was used for the able-bodied group, and the more impaired arm was used for the SCI group. Once inside the exoskeleton, the participant was strapped to the robot at the upper forearm and the hand.

Following these initial preparations, the user was then taken through calibration, training, and testing for each of the six control modes. All data were collected as the user started from a neutral position and performed an isometric contraction in the direction of a target presented on a visual display, while being held in place by the exoskeleton.

2) Calibration: To calibrate the system to detect the onset of contraction, the user performed a single isometric contraction in the direction of each target of the current control mode. Since the effort level of the user can greatly affect the classification [25], a calibration procedure was designed to control user effort level to be consistent. We chose to use the Teager-Kaiser Energy Operator (TKEO) to quantify the instantaneous power level of each EMG channel. This metric was chosen because it accounts for both the amplitude and frequency of the EMG waveform, both of which increase when

Authorized licensed use limited to: Fondren Library Rice University. Downloaded on April 10,2020 at 14:20:43 UTC from IEEE Xplore. Restrictions apply.

the muscle is active. It has also been demonstrated to be more robust for event detection than standard amplitude threshold techniques [26].

A 500 ms sample of the TKEO was captured while the user was at rest and while they performed an isometric contraction toward each target. The LDA classification algorithm was used to calculate the posterior probabilities of the user being either active or at rest. For able-bodied participants, a threshold active-state probability of 0.80 was set to indicate the onset of contraction, and a threshold rest-state probability of 0.80 was used between contractions to ensure that the user returned to a relaxed starting position. For SCI participants, these values were hand-tuned for better performance.

3) Training: To train the directional classifier, the user performed isometric contractions in the direction of each target to fit the classifier to the user's specific EMG activity. Visual targets were presented in a random order, and upon detection of the user's transition from a rest state to an active state, the full feature set was extracted from the last 200 ms of EMG data. The iterative LDA fitting and RFECV feature reduction algorithm was then performed.

Instead of defining a fixed amount of data to train the classifier, we chose to start with a low number of contractions (five per direction) and add training observations in increments of five per direction until the five-fold cross-validation score for classifier accuracy reached a minimum of 85% for all folds and the mean accuracy of the set was above 95%. If these criteria could not be achieved, the maximum number of training observations was capped at twenty per direction.

4) Testing: Classifier performance was tested under two conditions: with and without robot motion feedback. The first testing condition was *without* robot motion feedback. Users performed visually-prompted isometric contractions in the same manner as in training. There were ten repetitions per direction, presented in a random order. Following detection of the user's active state, the trained classifier used the selected features computed from the last 200 ms of EMG data to predict the direction of intended motion. The classifier prediction was recorded but not presented to the user in any form.

The purpose of the no-feedback condition, where the user was blind to the classifier predictions, was to ensure that they were not able to change their muscle activity in order to achieve better outcomes, thus allowing us to test the accuracy of the classifier more rigorously.

Testing *with* robot motion feedback functioned in the same manner as the without-feedback condition, except that the exoskeleton moved the user to the target predicted by the classifier immediately after each prediction. As this condition was more time consuming, there were only five repetitions per target, presented in a random order.

F. Data Analysis

For the testing condition *without* robot motion feedback, classifier performance was evaluated by first constructing a confusion matrix for each participant and each mode. The classification accuracy was then calculated from each confusion matrix as the sensitivity, or true positive rate, which is equivalent to the sum of the values on the main diagonal of the confusion matrix divided by the sum of all values. The average accuracy for the able-bodied group and for the SCI group was also calculated for each mode.

To determine whether the classifier performed better than chance, one-sided 95% confidence intervals for accuracy from random guessing were estimated for the binary (single-DoF) and four-class (multi-DoF) classification problems. Over 10,000 repetitions, with ten observations per class, classifier predictions were randomly generated from a discrete uniform distribution in order to calculate the confidence intervals for classification accuracy. Classification performance was considered unsuccessful if the accuracy was less than the upper bound of the random-chance confidence interval.

Regularization is often necessary to condition the fitting of a classifier. While conducting data analysis, it was determined that regularization was not appropriately applied to the covariance matrix inversion during the computation of the linear discriminant function. Therefore, this portion of the experimental code was rerun offline with automatic regularization. The corrected data were used in all subsequent data analysis and presented results.

In addition to basic classification accuracy, feature selection and its effect on performance were also evaluated. For each EMG feature, the frequency of selection by the RFECV algorithm was computed across all single-DoF modes and across both multi-DoF modes. Classifier training and testing was then re-run offline without RFECV for each participant and control mode: once using the entire feature set for each channel, and once using only one feature, the RMS, calculated on each channel.

For the testing condition *with* robot motion feedback, the same calculations of accuracy were performed, and the average accuracy for each group was calculated. Because there was very little data collected in this condition relative to the no feedback condition, more detailed analysis of the classification performance was not carried out.

III. Results

In this section we provide a more detailed breakdown of how classification accuracy compares between groups, and between single-DoF and multi-DoF modes, for the no feedback condition. Additionally, we show the number of training observations required to satisfy a certain predetermined cross-validation accuracy, which, like classification accuracy, is an important metric for evaluating the system's practical value. We then show the frequency with which specific features of the myoelectric signal were selected as useful inputs to the classifier. A comparison of classification accuracy using different methods of features selection and classification is presented for the discussion of variable performance across participants, and as a guide for possible future work. Finally, we present classifier performance for the robot motion feedback condition, as a demonstration of full real-time myoelectric control of the MAHI Exo-II.

A. Classification Accuracy: Able-Bodied Vs. SCI

The EMG-based classifier was able to classify the user's intended movement direction with a high degree of accuracy

Authorized licensed use limited to: Fondren Library Rice University. Downloaded on April 10,2020 at 14:20:43 UTC from IEEE Xplore. Restrictions apply.

TABLE II
CLASSIFICATION ACCURACY (%) BY PARTICIPANT, CONTROL MODE

	E-F/E	F-P/S	W-F/E	W-R/U	EF-Multi	WW-Multi
Able 1	100	100	100	100	97.5	95.0
Able 2	100	95.0	100	100	100	100
Able 3	100	100	100	100	77.5	90.0
Able 4	100	100	100	100	100	97.5
Able 5	100	100	95.0	100	87.5	87.5
Able 6	100	100	100	100	100	92.5
Able 7	100	100	100	100	67.5	57.5
Able 8	100	95.0	100	95.0	100	92.5
Able 9	100	100	100	100	95.0	100
Able 10	100	100	100	100	95.0	85.0
SCI 1	100	100	100	100	67.5	82.5
SCI 2	100	90.0	65.0	100	40.0	40.0
SCI 3	55.0	50.0	85.0	80.0	55.0	n/a
SCI 4	95.0	100	100	100	82.5	65.0
Able AVG (SD)	100 (0)	99.0 (2.10)	99.5 (1.58)	99.5 (1.58)	92.0 (11.2)	89.8 (12.4)
SCI AVG (SD)	87.5 (21.8)	85.0 (23.8)	87.5 (16.58)	95.0 (10.0)	61.3 (18.1)	62.5 (21.4)

for the able-bodied participants across modes. We found that the classifier was more accurate, on average, in the able-bodied group than the SCI group, though this difference was not uniform across participants and modes. Classifier performance during the no feedback condition is summarized in TABLE II, where classification accuracy is listed for all participants and all single-DoF and multi-DoF modes. Based on the random-chance confidence intervals, unsuccessful classification performance was defined as $<70.0\%$ for single-DoF modes and $<37.5\%$ for multi-DoF modes.

For the able-bodied participants, classification accuracy for the single-DoF modes reached 100.0% for most cases, and only dropped to 95.0% (one observation misclassified) in four cases. While the average accuracy for the two multi-DoF modes was near 90.0%, we still see higher variability in addition to lower average accuracy when compared to the single-DoF modes. For multi-DoF modes, the classification accuracy was at or above 85.0% for all but two participants. For one of those individuals, Able 7, the performance was notably lower—EF-Multi and WW-Multi accuracy was 67.5% and 57.5%, respectively—and it will be treated further in the discussion.

For the SCI participants, the classifier performance was varied, ranging from near the threshold of random chance to 100.0% for many single-DoF cases. For two participants, SCI 1 and SCI 4, the single-DoF classification accuracy was as high as it was for the able-bodied group. Single-DoF performance for participant SCI 2 was mostly equivalent to the able-bodied group, while for SCI 3 it was poor for all single-DoF modes when compared to the able-bodied group. This participant, SCI 3, was the most impaired of our SCI participants (ASIA A complete). Three individual cases (underlined in TABLE II) were found to have scored below the 70.0% threshold set

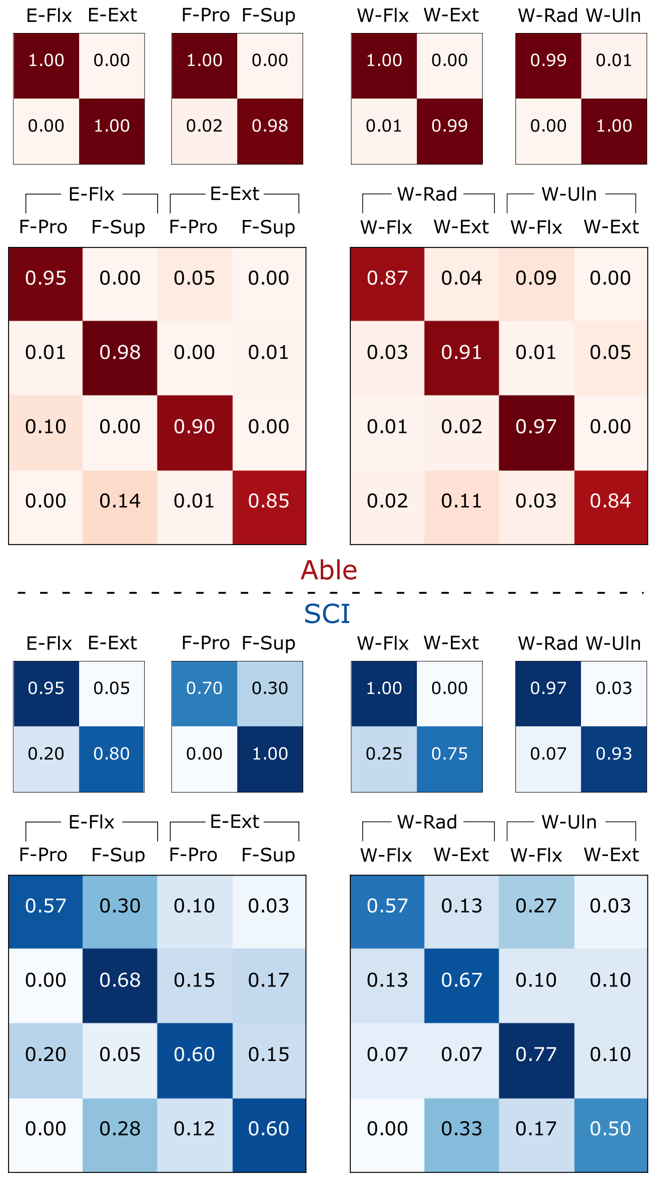

Fig. 5. Confusion matrices averaged across all able-bodied (top) and all SCI (bottom) participants, showing online classification performance (with corrected regularization). Each of the four single-DoF and two multi-DoF modes correspond to a 2-by-2 or 4-by-4 confusion matrix, respectively. Acronyms for intended motions are as follows: elbow flexion/extension (E-Flx/Ext), forearm pronation/supination (F-Pro/Sup), wrist flexion/extension (W-Flx/Ext), and wrist radial/ulnar deviation (W-Rad/Uln).

for being no better than random chance: SCI 2 W-Flx/Ext mode, and SCI 3 E-Flx/Ext and F-Pro/Sup modes. Multi-DoF performance for the SCI group was significantly lower than the able-bodied group average in nearly all cases. However, once again, SCI 1 and SCI 4 performed much better than SCI 2 and SCI 3. SCI participant 3 could not complete the final WW-Multi mode due to external timing constraints, and that data has simply been omitted from all reported individual and group results.

Confusion matrices averaged across all able-bodied and all SCI participants are shown in Fig. 5. Each row of a matrix corresponds to one of the possible directions, and the value

Authorized licensed use limited to: Fondren Library Rice University. Downloaded on April 10,2020 at 14:20:43 UTC from IEEE Xplore. Restrictions apply.

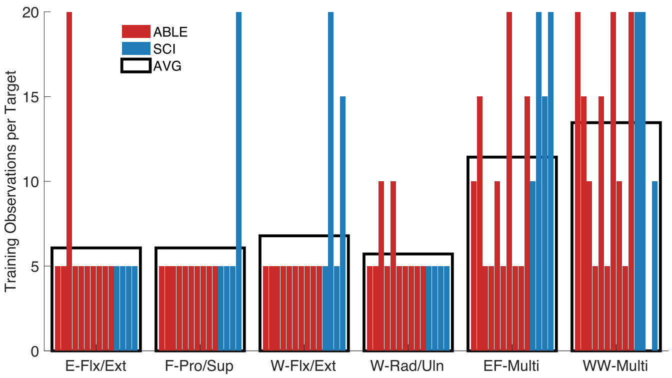

Fig. 6. Number of training observations required for the four single-DoF and two multi-DoF modes, with averages across participants shown in black outline. Control modes listed on the horizontal axis are: elbow flexion/extension (E-Flx/Ext), forearm pronation/supination (F-Pro/Sup), wrist flexion/extension (W-Flx/Ext), wrist radial/ulnar deviation (W-Rad/Uln), elbow-forearm multi-DoF (EF-Multi), and wrist multi-DoF (WW-Multi).

of each column within that row is the frequency - from 0 to 1 - at which the classifier predicted one of the directions from the same possible set of directions. Values on the main diagonal correspond to correct classifications, and all other values off the main diagonal correspond to misclassifications. Even within the lower-performing SCI group (bottom row, in blue), no target was consistently misclassified with greater frequency than it was correctly classified.

B. Training Observations Required

The number of training observations required to train the directional classifier is shown in Fig. 6. Training data was incrementally added until the cross-validation scores of the training set passed certain criteria, starting with 5 observations per directions and increasing by increments of 5 per direction until the maximum value of 20 observations per direction was reached. In the single-DoF modes, only the minimum value of 5 observations per direction was required 89% of the time. The amount of training data needed in the multi-DoF modes was more variable, averaging 12.4 observations per direction across participants. The instances that required more training data also exhibited lower classification accuracy, which is unsurprising given that more observations were acquired only when cross-validation scores of the training data were low.

C. Selected Features

EMG features used for movement classification were chosen by the Scikit-Learn toolbox's RFECV algorithm. As shown in Fig. 7, there was a noticeable difference in features selected for single-DoF movements versus multi-DoF movements. Namely, when operating in multi-DoF modes, fewer features were automatically selected, and the RMS and MAV features were chosen more frequently than the rest. For both single-DoF and multi-DoF modes, RMS and MAV were the only features chosen at a frequency greater than 50%.

D. Offline Comparison of Methods

Training and testing of the classifier were rerun offline for all participants and modes to compare our results against other

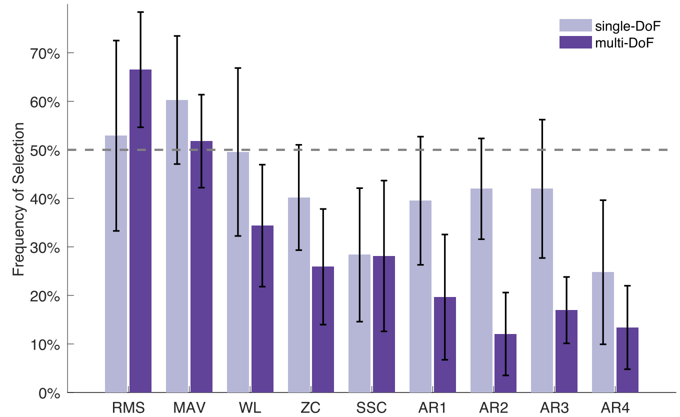

Fig. 7. Frequency of feature selection by recursive feature elimination with cross-validation across all participants (both able-bodied and SCI) and across all eight EMG channels, averaged across single-DoF and multi-DoF modes separately (bars show standard deviation). Features are root-mean-square (RMS), mean absolute value (MAV), waveform length (WL), number of zero crossings (ZC), number of slope sign changes (SSC), and autoregressive coefficients (AR1–4). RMS and MAV had a higher average selection rate (>50%) in both single-DoF and multi-DoF modes.

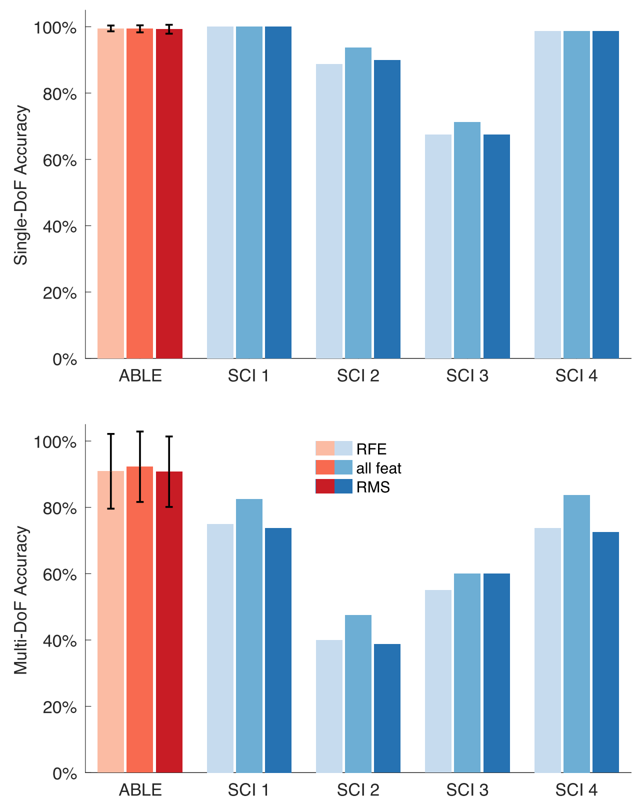

Fig. 8. Comparison of classification accuracy—separated into averages of single-DoF modes (top) and multi-DoF modes (bottom)—for different methods of feature selection and classification. For each subgroup of three bars, the methods used to generate the data, from left to right, are: *RFE* – recursive feature elimination with cross validation, our method; *all features* – using all possible features from all channels; and *RMS* – using only the root-mean-square value of each channel. The first grouping of three bars on the left shows the average scores across all able-bodied participants (error bars in black show standard deviation), and the remaining four groups show scores of individual SCI participants.

methods of feature selection. In Fig. 8, the effects of feature selection methods on classification accuracy are shown as averages across the single-DoF modes (top) and multi-DoF

Authorized licensed use limited to: Fondren Library Rice University. Downloaded on April 10,2020 at 14:20:43 UTC from IEEE Xplore. Restrictions apply.

TABLE III
CLASSIFICATION ACCURACY (%) BY CONTROL MODE, WITH ROBOT MOTION FEEDBACK

	E-F/E	F-P/S	W-F/E	W-R/U	EF-Multi	WW-Multi
Able AVG (SD)	100 (0)	100 (0)	100 (0)	100 (0)	88.5 (9.4)	93.0 (9.2)
SCI AVG (SD)	95.0 (10.0)	100 (0)	95.0 (10.0)	85.0 (23.8)	58.8 (32.5)	73.3 (20.2)

modes (bottom). The data are also presented as an average for the able-bodied group, since the effects on the SCI participants are of more interest.

Accuracy was highest, on average – uniformly, within the SCI group – when *all* features were used. When the feature set was reduced to include only RMS, the classification accuracy was very similar to that of the REFCV algorithm. It should be noted that results from these *post hoc* decisions are not valid predictions of which method will perform better when implemented online, as would be the case when triggering for robotic rehabilitation, but provide additional information about the linear separability of this specific data set.

E. Testing With Robot Motion Feedback

Classification testing for each mode was always done under two conditions: first, without robot motion feedback, and then, with robot motion feedback, i.e., with the robot moving to the target predicted by the classifier. The feedback condition (FB) testing generated a smaller data set than that of the no feedback condition (5 observations per direction, as opposed to 10). The resulting classification accuracy, presented in TABLE III, is qualitatively similar to that seen during the no-feedback condition.

IV. DISCUSSION

The performance of this EMG-based classifier, and, more generally, of this real-time myoelectric control interface, was found to be as good as expected for the able-bodied population, with averages of single-DoF classification accuracy over 99%, and averages of multi-DoF classification accuracy near 90% (a reasonable threshold for clinical usability [14].)

For the SCI participants, the results encourage the further development of myoelectric control interfaces for rehabilitation robots. The average classification accuracy for the single-DoF control modes ranged from 85.0% to 95.0%, and for the multi-DoF modes it was just above 60%. Given the severity of the impact of a cervical level spinal injury on motor function, it is not surprising that the performance of the classifier for the SCI group does not match that of the able-bodied group. The ability to accurately classify movement intent for some SCI participants, especially in the single-DoF modes, is evidence of useful information in the myoelectric signal for control of a robotic rehabilitation device at that joint.

The use of a variably-sized training data set, Fig. 6, was effective in reducing training time where it was possible – the vast majority of the single-DoF classifiers were trained on the predetermined minimum number of 5 observations per direction. It was also effective in reaching the desired cross-validation accuracy to terminate training for many of the cases where the minimum-size training set was insufficient.

Using the RFECV algorithm to select a subset of the possible features revealed a preference for the root-mean-square (RMS) and mean absolute value (MAV) of the EMG window for classifying intended direction, specifically in the multi-DoF case, Fig. 7. This suggests that when designing a classifier for any similar motor task in the future, inclusion of either one or both of these features would be advisable.

In contrast, the offline comparison of feature selection methods, illustrated in Fig. 8, showed a consistent increase in accuracy across participants and modes when the entire possible feature set was used, as compared to the recursive feature elimination algorithm. The offline accuracy was boosted by giving the classifier access to all the information in the full feature set, while not being negatively affected by the higher dimension of the feature space. While we expected feature reduction to prevent overfitting and lead to higher performance, this was not what we observed in the offline comparison. Additionally, we found that using RMS as the only feature computed on each channel was comparable to using recursive feature elimination, suggesting that the more computationally intensive recursive feature elimination algorithm can be replaced with a simpler choice in future work. It is also interesting to note that RFE algorithm is the only one of these feature reduction methods that is participant-specific, yet it did not out-perform the other methods. These findings are consistent with the studies by Lorrain *et al.* [19] and Huang *et al.* [20], which found the combination of time domain and autoregressive features (and RMS, in [20]) to perform the best in classification schemes for myoelectric upper-limb prostheses.

Across the different methods compared in Fig. 8, the accuracy for certain participants in certain control modes remained markedly lower than others in their respective participant group, suggesting that something may set them apart. The first two single-DoF modes (E-Flx/Ext and F-Pro/Sup) for SCI participant 3—the most impaired participant—remained below 70% accuracy, and the two multi-DoF modes for SCI participant 2 remained at or below 50% accuracy. A "low-performer" was also observed in the able-bodied group: the two multi-DoF modes for Able-bodied participant 7 remained below 75% accuracy for all methods tried, setting them apart from the accuracy of the other able-bodied participants. Able-bodied participant 7 scored 100% on all single-DoF modes, suggesting that there may have been some difficulty with the multi-DoF modes either at the level of motor coordination or at the cognitive level; however, further investigation is required to identify the root cause.

Though limited studies on the real-time performance of such classification algorithms exist, particularly for SCI, there are a few that provide a basis of comparison to our study. Lu *et al.* [16] used a linear Bayes classifier, four EMG channels, and a similar feature set, and showed that the classifier recognized six possible hand motions intended by the user and controlled the corresponding movements of

Authorized licensed use limited to: Fondren Library Rice University. Downloaded on April 10,2020 at 14:20:43 UTC from IEEE Xplore. Restrictions apply.

a hand exoskeleton. For eight neurologically intact participants, the average classification accuracy was 98.1%. Two individuals with cervical level SCI participated, for whom the average classification accuracy was 90.0%. We achieved this level of performance with able bodied participants, and with a subset of our SCI participants. In a study with amputees, Englehart *et al.* [27] produced a similar LDA classifier to the WW-Multi mode, where they were able to achieve 94% accuracy using an *offline*, continuous classification scheme. While our scheme required an average of 13.5 observations per direction for training the WW-Multi mode, in [27], a constant 10 observations per direction were collected. These comparisons are difficult to make, however, since the specific details of the methods and target populations used are quite different from our own, and the sample sizes are so small. Yet, with a lack of more suitable alternatives, such studies at least provide a point of reference for the possible accuracy that could be achieved in multi-class classification of EMG patterns for both able-bodied and SCI individuals.

Techniques from control of prostheses and complex robotic systems [28]–[30] show promise for application to robotic rehabilitation. For example, simultaneous control of multiple degrees of freedom can be achieved through regression [28], [29], instead of classification, along with higher-density placement of EMG electrodes. Our objective in this paper was to demonstrate myoelectric control of our robotic exoskeleton with the incomplete cervical SCI population, as compared to able-bodied individuals. Given that our participants are impaired in their ability to generate muscle activations, additional challenges must be overcome to translate these methods to rehabilitation applications. Regarding real-time classification for multi-DoF control of prostheses, results from [30] indicate that the topology of the classifier should be examined in the interest of improved accuracy and scalability of multi-DoF control. Here, offline classification accuracy for 6 single-DoF and 20 multi-DoF movements, plus rest, averaged across 17 reached as high as 93.7% (SD = 2.5%) using LDA with other topologies.

Analyzing classifier performance in the robot motion feedback condition serves both to validate the full closed-loop EMG-controlled exoskeleton system and to study the effect of the robot motion feedback separately from the recognition of intent. Notably, during this phase of the experiment, participants instinctively tried to make use of their new knowledge of the classifier predictions and to alter their muscle activity to achieve more correct predictions. This result is quite encouraging for those who wish to use EMG in a rehabilitation training protocol.

The results of testing with robot motion feedback are only preliminary and come from a relatively small data set, so further study is needed to see how well users of this system learn to adapt their myoelectric activity. How such a myoelectric training program could be utilized for robotic rehabilitation is a particularly interesting question that is starting to garner some attention [31]. Myoelectric control of rehabilitation robots could lead to future opportunities for therapists to train certain muscle coordination strategies and reduce maladaptive muscle activation patterns [12].

V. Conclusions

In this paper, the design of a myoelectric control interface for an upper-limb exoskeleton was presented and evaluated with able-bodied and SCI individuals. The system was able to classify intended movement direction with a high degree of accuracy for able-bodied users across single and multi-DoF control modes, while the classification performance was more variable with SCI users, but still achieved high accuracy with some frequency across control modes. The use of EMG to control an exoskeleton in real time shows promise for translation from the unimpaired population to the target population, SCI, particularly with simpler single-DoF directional classification tasks.

References

[1] *National Spinal Cord Injury Statistical Center, Facts and Figures at a Glance*, Univ. Alabama Birmingham, Birmingham, AL, USA, 2019.

[2] J. W. McDonald and C. Sadowsky, “Spinal-cord injury,” *Lancet*, vol. 359, no. 9304, pp. 417–425, 2002. [Online]. Available: http://www.sciencedirect.com/science/article/pii/S0140673602076031

[3] D. J. Reinkensmeyer, J. L. Emken, and S. C. Cramer, “Robotics, motor learning, and neurologic recovery,” *Annu. Rev. Biomed. Eng.*, vol. 6, no. 1, pp. 497–525, Aug. 2004.

[4] N. Hogan *et al.*, “Motions or muscles? Some behavioral factors underlying robotic assistance of motor recovery,” *J. Rehabil. Res. Develop.*, vol. 43, no. 5, p. 605, 2006.

[5] A. U. Pehlivan, D. P. Losey, C. G. Rose, and M. K. O’Malley, “Maintaining subject engagement during robotic rehabilitation with a minimal assist-as-needed (mAAN) controller,” in *Proc. Int. Conf. Rehabil. Robot. (ICORR)*, Jul. 2017, pp. 62–67.

[6] D. A. E. Bolton, J. H. Cauraugh, and H. A. Hausenblas, “Electromyogram-triggered neuromuscular stimulation and stroke motor recovery of arm/hand functions: A meta-analysis,” *J. Neurol. Sci.*, vol. 223, no. 2, pp. 121–127, Aug. 2004.

[7] M. F. Levin and E. Panturin, “Sensorimotor integration for functional recovery and the Bobath approach,” *Motor Control*, vol. 15, no. 2, pp. 285–301, Apr. 2011.

[8] J. W. Krakauer, “Motor learning: Its relevance to stroke recovery and neurorehabilitation,” *Current Opinion Neurol.*, vol. 19, no. 1, pp. 84–90, Feb. 2006.

[9] N. Jiang, D. Falla, A. d’Avella, B. Graimann, and D. Farina, “Myoelectric control in neurorehabilitation,” *Crit. Rev. Biomed. Eng.*, vol. 38, no. 4, pp. 381–391, 2010.

[10] C. W. Moss, K. L. Kilgore, and P. H. Peckham, “A novel command signal for motor neuroprosthetic control,” *Neurorehabilitation Neural Repair*, vol. 25, no. 9, pp. 847–854, Nov. 2011, doi: 10.1177/1545968311410067.

[11] E. Heald, R. Hart, K. Kilgore, and P. H. Peckham, “Characterization of volitional electromyographic signals in the lower extremity after motor complete spinal cord injury,” *Neurorehabilitation Neural Repair*, vol. 31, no. 6, pp. 583–591, Jun. 2017.

[12] B. Cesqui, P. Tropea, S. Micera, and H. Krebs, “EMG-based pattern recognition approach in post stroke robot-aided rehabilitation: A feasibility study,” *J. NeuroEngineering Rehabil.*, vol. 10, no. 1, p. 75, 2013.

[13] B. Hudgins, P. Parker, and R. N. Scott, “A new strategy for multifunction myoelectric control,” *IEEE Trans. Biomed. Eng.*, vol. 40, no. 1, pp. 82–94, 1993.

[14] E. Scheme and K. Englehart, “Electromyogram pattern recognition for control of powered upper-limb prostheses: State of the art and challenges for clinical use,” *J. Rehabil. Res. Develop.*, vol. 48, no. 6, p. 643, 2011.

[15] K. Englehart and B. Hudgins, “A robust, real-time control scheme for multifunction myoelectric control,” *IEEE Trans. Biomed. Eng.*, vol. 50, no. 7, pp. 848–854, Jul. 2003.

[16] Z. Lu, X. Chen, X. Zhang, K.-Y. Tong, and P. Zhou, “Real-time control of an exoskeleton hand robot with myoelectric pattern recognition,” *Int. J. Neural Syst.*, vol. 27, no. 5, Aug. 2017, Art. no. 1750009.

[17] R. A. R. C. Gopura and K. Kiguchi, “EMG-based control of an exoskeleton robot for human forearm and wrist motion assist,” in *Proc. IEEE Int. Conf. Robot. Autom. (ICRA)*, May 2008, pp. 731–736.

Authorized licensed use limited to: Fondren Library Rice University. Downloaded on April 10,2020 at 14:20:43 UTC from IEEE Xplore. Restrictions apply.

[18] N. Palastanga, D. Field, and R. Soames, *Anatomy and Human Movement: Structure and Function*. London, U.K.: Avon, 1989.

[19] T. Lorrain, N. Jiang, and D. Farina, "Influence of the training set on the accuracy of surface EMG classification in dynamic contractions for the control of multifunction prostheses," *J. NeuroEng. Rehabil.*, vol. 8, no. 1, p. 25, 2011.

[20] Y. Huang, K. B. Englehart, B. Hudgins, and A. D. C. Chan, "A Gaussian mixture model based classification scheme for myoelectric control of powered upper limb prostheses," *IEEE Trans. Biomed. Eng.*, vol. 52, no. 11, pp. 1801–1811, Nov. 2005.

[21] L. H. Smith, L. J. Hargrove, B. A. Lock, and T. A. Kuiken, "Determining the optimal window length for pattern recognition-based myoelectric control: Balancing the competing effects of classification error and controller delay," *IEEE Trans. Neural Syst. Rehabil. Eng.*, vol. 19, no. 2, pp. 186–192, Apr. 2011.

[22] J. Liu, X. Li, G. Li, and P. Zhou, "EMG feature assessment for myoelectric pattern recognition and channel selection: A study with incomplete spinal cord injury," *Med. Eng. Phys.*, vol. 36, no. 7, pp. 975–980, Jul. 2014.

[23] K. D. Fitle, A. U. Pehlivan, and M. K. O'Malley, "A robotic exoskeleton for rehabilitation and assessment of the upper limb following incomplete spinal cord injury," in *Proc. IEEE Int. Conf. Robot. Autom. (ICRA)*, Seattle, WA, USA, May 2015, pp. 4960–4966.

[24] B. Freriks and H. Hermens, "European recommendations for surface electromyography," *Roessingh Res. Develop.*, vol. 8, no. 2, pp. 13–54, 1999.

[25] B. Atoufi, E. N. Kamavuako, B. Hudgins, and K. Englehart, "Classification of hand and wrist tasks of unknown force levels using muscle synergies," in *Proc. 37th Annu. Int. Conf. IEEE Eng. Med. Biol. Soc. (EMBC)*, Aug. 2015, pp. 1663–1666.

[26] S. Solnik, P. Rider, K. Steinweg, P. DeVita, and T. Hortobágyi, "Teager–Kaiser energy operator signal conditioning improves EMG onset detection," *Eur. J. Appl. Physiol.*, vol. 110, no. 3, pp. 489–498, Oct. 2010.

[27] K. Englehart, B. Hudgins, P. A. Parker, and M. Stevenson, "Classification of the myoelectric signal using time-frequency based representations," *Med. Eng. Phys.*, vol. 21, nos. 6–7, pp. 431–438, Jul. 1999.

[28] N. Jiang, H. Rehbaum, I. Vujaklija, B. Graimann, and D. Farina, "Intuitive, online, simultaneous, and proportional myoelectric control over two degrees-of-freedom in upper limb amputees," *IEEE Trans. Neural Syst. Rehabil. Eng.*, vol. 22, no. 3, pp. 501–510, May 2014.

[29] M. Ison, I. Vujaklija, B. Whitsell, D. Farina, and P. Artemiadis, "High-density electromyography and motor skill learning for robust long-term control of a 7-DoF robot arm," *IEEE Trans. Neural Syst. Rehabil. Eng.*, vol. 24, no. 4, pp. 424–433, Apr. 2016.

[30] M. Ortiz-Catalan, B. Hkansson, and R. Brnemark, "Real-time and simultaneous control of artificial limbs based on pattern recognition algorithms," *IEEE Trans. Neural Syst. Rehabil. Eng.*, vol. 22, no. 4, pp. 756–764, Jul. 2014.

[31] M. Semprini, A. V. Cuppone, I. Delis, V. Squeri, S. Panzeri, and J. Konczak, "Biofeedback signals for robotic rehabilitation: Assessment of wrist muscle activation patterns in healthy humans," *IEEE Trans. Neural Syst. Rehabil. Eng.*, vol. 25, no. 7, pp. 883–892, Jul. 2017.

Authorized licensed use limited to: Fondren Library Rice University. Downloaded on April 10,2020 at 14:20:43 UTC from IEEE Xplore. Restrictions apply.